# Numerical Simulation of Turbulent Incompressible and Compressible Flows Over Rough Walls

**Petr Louda, Jaromír Příhoda, and Karel Kozel**

## 1 Introduction

Wall roughness affects flow characteristics practically in all technical applications. In internal flows, the height of rough elements should be much smaller than the thickness of the shear layer (so called distributed roughness) and its influence on the flow cannot be directly simulated. Instead a model of rough wall is needed.

Wall roughness influences the flow structure only in the vicinity of the wall. The effect of wall roughness on the velocity profile can be expressed by the shift of the mean velocity profile in the logarithmic part of the wall region.

In this work, the SST $k$-$\omega$ model is used to compute two cases of incompressible flows over rough walls, and one case of compressible flow through a turbine cascade. Also Spalart-Allmaras model modified for rough walls [3] is tested on flat plate flow, but its results are not encouraging. Further, the same aproach as for the SST model is used for explicit algebraic Reynolds stress (EARSM) model by Wallin and Hellsten [5, 13]. This model uses $k$-$\omega$ system of equations very similar to SST one, and results show the effect of roughness can be incorporated with similar reliability as in the SST model. Results are compared with measurements and the effect of wall roughness shown by comparison with computation for smooth walls.

P. Louda (✉), and J. Příhoda
Institute of Thermomechanics v.v.i., Czech Academy of Sciences, Dolejškova 5, 182 00 Praha 8, Czech Republic,
e-mail: louda@it.cas.cz, prihoda@it.cas.cz

K. Kozel
Department of Technical Mathematis, Faculty of Mechanical Engineering, Czech Technical University in Prague, Karlovo nám. 13, 121 35 Praha 2, Czech Republic,
e-mail: karel.kozel@fs.cvut.cz

C. Clavero et al. (eds.), *BAIL 2010 – Boundary and Interior Layers, Computational and Asymptotic Methods*, Lecture Notes in Computational Science and Engineering 81,
DOI 10.1007/978-3-642-19665-2_17, 

## 2 Mathematical and Numerical Model

The mathematical model of compressible turbulent flow is based on the Favre averaged Navier–Stokes equations in 2D case

$$\frac{\partial W}{\partial t} + \frac{\partial F_i}{\partial x_i} = \frac{\partial R_i}{\partial x_i},\ (i = 1,\ 2) \tag{1}$$

$$W = \begin{bmatrix} \rho \\ \rho u_1 \\ \rho u_2 \\ e \end{bmatrix},\ F_i = \begin{bmatrix} \rho u_i \\ u_i \rho u_1 + p\delta_{i1} \\ u_i \rho u_2 + p\delta_{i2} \\ u_i(e+p) \end{bmatrix},\ R_i = \begin{bmatrix} 0 \\ \sigma_{i1} - t_{i1} \\ \sigma_{i2} - t_{i2} \\ (\sigma_{ij} - t_{ij})u_j - q_i - q_i^t \end{bmatrix},$$

where $\rho$ is mean density, $u_i$ mean velocity vector, $p$ mean static pressure, $\delta_{ij}$ is the Kronecker delta, $\sigma_{ij}$ tensor of viscous stress, $e$ mean total energy per unit volume and $q_i$ heat flux vector. A state equation of perfect gas is assumed. The tensor $t_{ij}$ is the Reynolds stress tensor and $q_i^t$ turbulent heat flux. These terms are approximated by a turbulence model. For incompressible fluid flows, the corresponding system of simplified Navier–Stokes equations is used instead of the above system with $\rho = const$.

### 2.1 Turbulence Model

The eddy viscosity SST (Shear Stress Transport) model by Menter [4], defines the Reynolds stress tensor by eddy viscosity $\mu_t$

$$t_{ij} = -\mu_t 2S_{ij} + \frac{2}{3}\rho k\delta_{ij},\ \mu_t = \frac{a_1 \rho k}{\max(a_1\omega, |\Omega| F_2)},\quad a_1 = 0.31 \tag{2}$$

where $k$ is turbulent energy, $\omega$ specific dissipation rate and $S_{ij}$ and $\Omega_{ij}$ are the strain rate tensor and the rotation tensor respectively. $|\Omega| = (\Omega_{ij}\Omega_{ij})^{1/2}$ is the absolute value of the rotation tensor. The function $F_2$ activates the Bradshaw hypothesis for the Reynolds shear stress $t_{12} = a_1 \rho k$, see [4].

The EARSM model by Wallin [13] can be expressed in terms of dimensionless anisotropy tensor $a_{ij}$ as

$$\begin{aligned} t_{ij} &= a_{ij}\rho k + \frac{2}{3}\rho k\delta_{ij}, \\ a_{ij} &= \beta_1 \tau S_{ij} \\ &\quad + \beta_3 \tau^2 (\Omega_{ik}\Omega_{kj} - II_\Omega \delta_{ij}/3) + \beta_4 \tau^2 (S_{ik}\Omega_{kj} - \Omega_{ik}S_{kj}) \\ &\quad + \beta_6 \tau^3 (S_{ik}\Omega_{kl}\Omega_{lj} + \Omega_{ik}\Omega_{kl}S_{lj} - 2IV\delta_{ij}/3) \\ &\quad + \beta_9 \tau^4 (\Omega_{ik}S_{kl}\Omega_{lm}\Omega_{mj} - \Omega_{ik}\Omega_{kl}S_{lm}\Omega_{mj}), \end{aligned} \tag{3}$$

where $\tau$ is turbulent time scale and $S_{ij}$, $\Omega_{ij}$ are strain rate and rotation tensors, respectively. The invariants $II_\Omega$, $IV$ formed by $S_{ij}$, $\Omega_{ij}$ are given in Hellsten [5] as well as coefficients $\beta$. The original version of model by Wallin [13] has slightly different coefficients $\beta$. It should be noted, that only $\beta_1$, $\beta_4$ should be non-zero in a 2D mean flow. However, due to the necessary approximate explicit solution of the algebraic stress model, not all remaining coefficients are exactly zero in 2D. In this work the general 3D form of the model is used without regard to 2D geometrical configuration.

The turbulent heat flux is approximated by

$$q_i^t = q_i \frac{Pr}{\mu} \frac{\mu_t}{Pr_t}, \tag{4}$$

where the turbulent Prandtl number $Pr_t = 0.91$ and $\mu_t$ is defined using the linear part of the Reynolds stress tensor in the case of EARSM model.

Both turbulence models use the $k$-$\omega$ system of equations to estimate turbulent scales

$$\begin{aligned} \frac{D\rho k}{Dt} &= -t_{ij}\frac{\partial u_i}{\partial x_j} - \beta^* \rho k \omega + \frac{\partial}{\partial x_j}\left[(\mu + \sigma_k \mu_t)\frac{\partial k}{\partial x_j}\right], \\ \frac{D\rho \omega}{Dt} &= -\gamma \frac{\omega}{k} t_{ij}\frac{\partial u_i}{\partial x_j} - \beta \rho \omega^2 + \frac{\partial}{\partial x_j}\left[(\mu + \sigma_\omega \mu_t)\frac{\partial \omega}{\partial x_j}\right] + \rho \frac{\sigma_d}{\omega}\frac{\partial k}{\partial x_j}\frac{\partial \omega}{\partial x_j} \end{aligned} \tag{5}$$

where the derivative $D\cdot/Dt \equiv \partial\cdot/\partial t + \partial(u_j\cdot)/\partial x_j$. For the coefficients $\beta^*$, $\sigma_k$, $\gamma$, $\beta$, $\sigma_\omega$, $\sigma_d$ in the SST or EARSM model see [4] and [5] respectively.

## 2.2 Roughness Model

The effect of wall roughness on the velocity profile can be expressed by the shift of the mean velocity profile in the logarithmic part of the wall region $\Delta u$. According to Nikuradse [9] it is expressed using the equivalent sand grain roughness $k_s$

$$\frac{\Delta u}{u_\tau} = \frac{1}{\kappa} \ln \frac{u_\tau k_s}{\nu} - 3, \quad \kappa = 0.41 \tag{6}$$

where $u_\tau$ is the friction velocity. The velocity shift occurs also in a $k$-$\omega$ turbulence model if it is integrated up to the wall with wall value of $\omega$ which is not large enough. Wilcox [12] proposed value of $\omega$ on the rough wall in the form

$$\omega_w = \frac{u_\tau^2}{\nu} S_R, \quad S_R = \begin{cases} [50/\max(k_s^+, k_{\mathrm{smin}}^+)^2] & \text{for } k_s^+ < 25 \\ 100/k_s^+ & \text{for } k_s^+ \geq 25 \end{cases} \tag{7}$$

The smooth regime is reached for values $k_s^+ < 4$. Hellsten [5] observed that the wall shear stress is very sensitive to the value $k_{\text{smin}}^+$ which determines the smooth regime. To remove such dependence he proposed the following relation

$$k_{\text{smin}}^+ = \min[2.4(\Delta y_1^+)^{0.85}, 8] \tag{8}$$

where $\Delta y_1^+$ is the thickness of the grid cell next to the wall. The boundary condition given by (7) and (8) is used for the SST as well as the EARSM turbulence model.

The SST model is further modified according to Hellsten and Laine [6] by introduction of the function $F_3$ to prevent the activation of the SST limiter in the roughness layer

$$\mu_t = \frac{a_1 \rho k}{\max(a_1 \omega, |\Omega| F_2 F_3)}, \quad F_3 = 1 - \tanh\left(\frac{150\nu}{\omega y^2}\right)^4 \tag{9}$$

The function $F_3$ is equal zero near the wall and unity elsewhere.

## 3 Numerical Method

The system of governing equations is solved by the implicit upwind finite volume method. The cell centered finite volume method with quadrilateral finite volumes is applied for spatial discretization. The inviscid flux in the case of compressible flow is defined using the AUSM U-splitting [7]. A higher order of accuracy is achieved by the MUSCL interpolation in the directions of grid lines using the van Leer limiter. In the case of the steady incompressible flow an artificial compressibility method is used which consists of adding a pressure time derivative into the continuity equation

$$\frac{1}{a^2}\frac{\partial p}{\partial t} + \frac{\partial u_i}{\partial x_i} = 0, \tag{10}$$

where $a$ is a positive constant parameter chosen for good convergence to a steady state. In this work $a$ is approximately equal to the maximum velocity. The inviscid flux is discretized using the third order van Leer upwind interpolation in the direction of grid lines without limiter. The discretization of diffusive fluxes is central. The approximation of cell face derivatives needed in diffusive terms uses quadrilateral dual finite volumes constructed over each face of primary finite volume. The time integration uses the backward Euler implicit scheme. The non-linear discrete equations are linearized using the Newton method. The resulting block 5-diagonal system of algebraic equations is solved using block relaxation method with direct tri-diagonal solver for selected family of grid lines [2, 8].

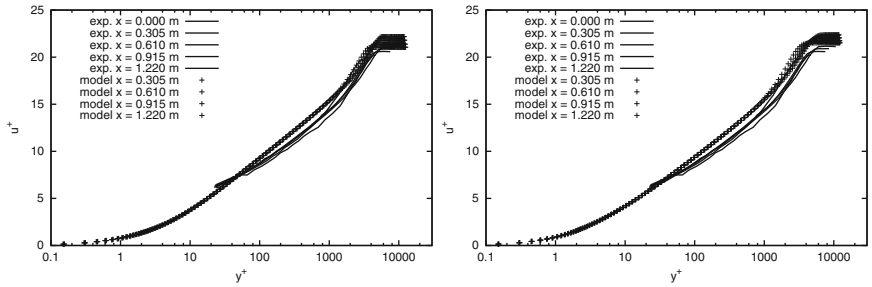


**Fig. 1** Flat-plate flow, mean velocity profiles (*left*: SST model, *right*: EARSM model)

## 4 Computational Results

### *4.1 Flat Plate Flow*

The roughness model was tested on the incompressible constant-pressure boundary layer. The measurement data are taken from Pimenta, Moffat and Kays [10]. The flat plate was covered by tightly packed spheres of 1.27 mm diameter, which corresponds to the equivalent sand roughness $k_s = 0.683$ mm. Numerical results are compared with experimental data for the free-stream velocity $U_e = 39.7$ m/s. Figure 1 shows mean velocity profiles in non-dimensional coordinates and Fig. 2 the distribution of the boundary layer thickness, here including also results of Spalart-Allmaras one-equation model. The computational results are in a good agreement with measurement, except for Spalart-Allmaras model which under-predicts wall shear stress.

### *4.2 Flow Over Ramp*

Here an incompressible flow in a channel with ramp on the bottom wall according to measurements of Song and Eaton [11] is considered. The sketch of the channel with a smoothly contoured ramp formed by a circular arch with a radius of 127 mm is given in Fig. 3. The bottom wall was covered with 36-grit sandpaper from 1.3 m up-stream of the ramp to the ramp trailing edge. The wall roughness is characterized by the equivalent sand roughness $k_s = 2.4$ mm. Numerical simulation was carried out for the free stream velocity $U_e = 20$ m/s.

For smooth ramp, both SST and EARSM model give recirculation zone twice as long as measured (approx. 85 mm vs. 43 mm). In the case of rough ramp, the reattachment point is predicted nearly exactly. The separation point is not given exactly in the reference. Figure 4 shows profiles of mean velocity and shear Reynolds stress

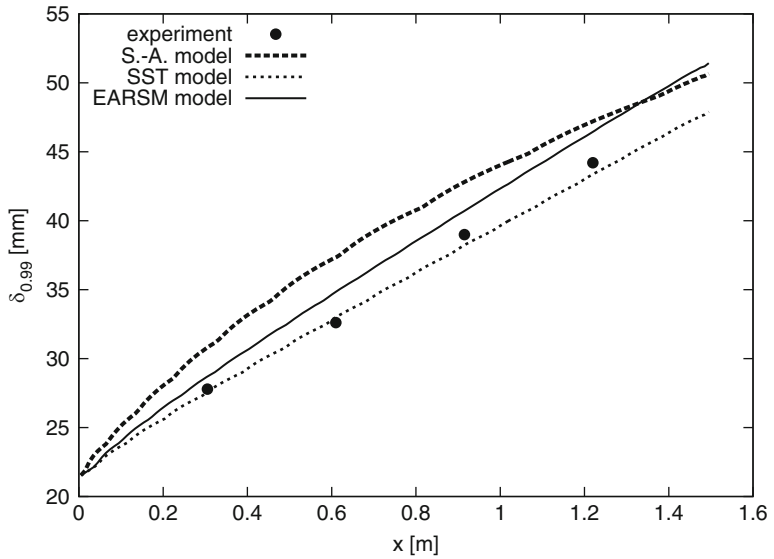


**Fig. 2** Flat-plate flow, boundary layer thickness

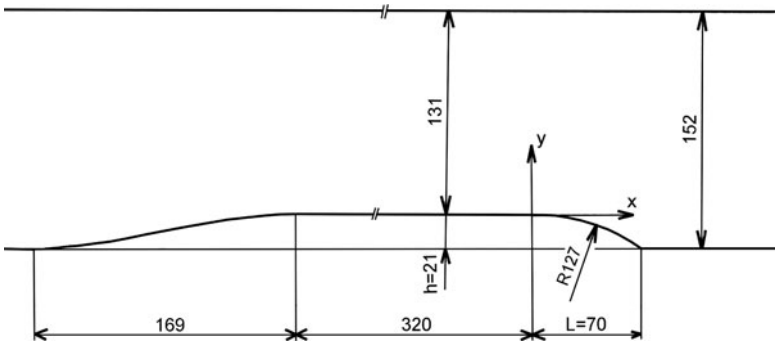


**Fig. 3** Geometry of the circular ramp

compared to measurement [11]. The agreement with measurement is again better for the rough ramp than for smooth one (not shown).

## *4.3 Flow Through a Turbine Cascade*

Finally, a subsonic flow through VS33 turbine blade cascade with the chord length $b = 75\,\text{mm}$ is considered. Two similar regimes are chosen which differ mainly by the roughness of the blade from measurements carried out by Ulrych et al. [1]. The value of $k_s = 0\,\text{mm}$ was considered for smooth blades, whereas for rough

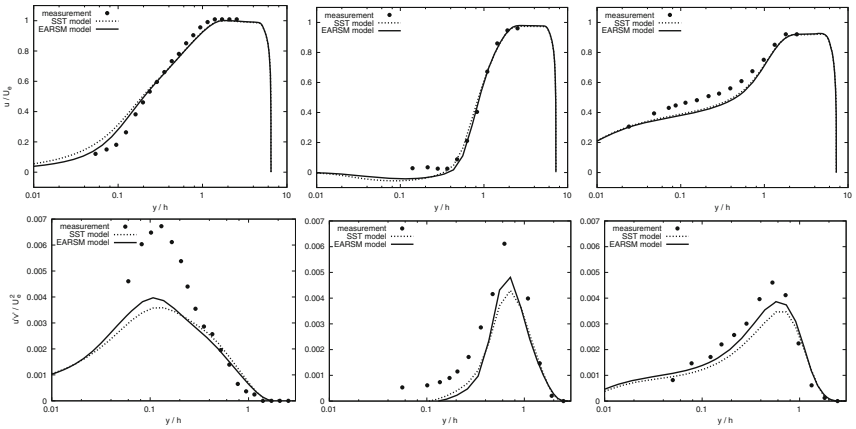


**Fig. 4** Rough ramp: mean velocity and Reynolds shear stress in the middle of the ramp, at the end of the ramp, and 3 ramp lengths downstream (from left to right)

blades covered with carborundum particles with $Ra = 30\,\mu\text{m}$ the corresponding equivalent sand roughness $k_s = 0.174\,\text{mm}$ was used. The smooth regime is characterized by the isentropic outlet Mach number $M_{2is} = 0.88$, the Reynolds number $Re_{2is} = 8.4 \cdot 10^5$, and the angle of attack $\alpha_1 = 0°$ while the rough regime by values $M_{2is} = 0.90,\ Re_{2is} = 8.8 \cdot 10^5,\ \alpha_1 = 6°$. In both cases, the total temperature $T_0 = 293\ K$ and ratio of specific heats $\gamma = 1.4$ was considered.

The pressure and shear stress distribution on smooth and rough blades are shown in Fig. 5. There is no significant difference between SST and EARSM models. The roughness, as expected, influences mainly shear stress and not much the static pressure on the blade. The energy loss coefficient $\xi$ was evaluated using the Laval numbers $\lambda_2,\ \lambda_{2is}$ according to relations

$$\xi = 100(1 - \lambda_2^2/\lambda_{iso2}^2),$$
$$\lambda_2^2 = \frac{\gamma+1}{2}\left[1 + \frac{\gamma-1}{2}M_{2is}^2\right]^{-1} M_{2is}^2, \quad \lambda_{iso2}^2 = \frac{\gamma+1}{\gamma-1}\left[1 - \left(\frac{p_2}{p_0}\right)^{\frac{\gamma-1}{\gamma}}\right] \tag{11}$$

where $p_2$ and $p_0$ are mean values of the static pressure behind the cascade and the total pressure obtained from mean mass and momentum fluxes. The overview of the loss coefficient is given in the Table 1. Although loss coefficients predicted by the both turbulence models differ, the wall roughness characterized by the parameter $Ra = 30\,\mu\text{m}$ causes always approximately equal increase in the loss coefficient by 62%–65%. The difference between measured and calculated losses for smooth blades could be caused by the fact that the prediction was carried out for turbulent flow only, without considering the laminar part. This difference is negligible for rough blades, as the laminar/turbulent transition occurs very early.

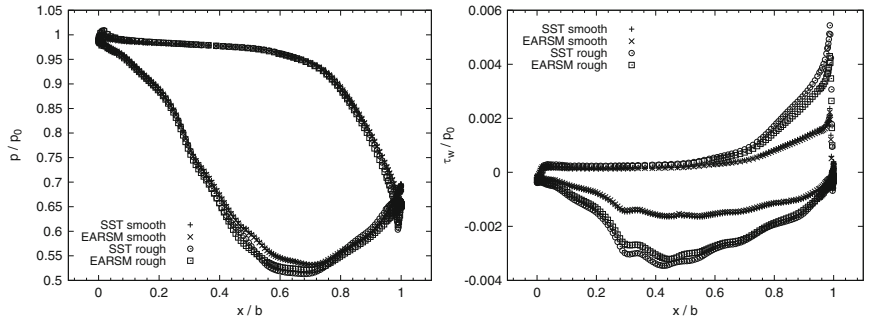


**Fig. 5** Static pressure and friction on the blade

**Table 1** Kinetic energy loss coefficient

| | Measurement | SST model | EARSM model |
|---|---|---|---|
| Smooth blade | 2.2% | 4.3% | 3.7% |
| Rough blade | 6.6% | 7.0% | 6.1% |
| Increase by roughness | 200% | 62% | 65% |

## 5 Conclusions

The prescription of boundary conditions directly on the rough wall was tested in the framework of SST and EARSM turbulence models. Based on the considered cases, the roughness model developed for $k$-$\omega$ eddy viscosity model can be used in the EARSM model as well. This makes possible future 3D simulations with EARSM model and rough walls, where eddy viscosity models typically fail in capturing secondary flows. In the turbine cascade simulation the accounting for wall roughness causes same change in loss coefficient for both turbulence models, although this parameter is sensitive and different for both models. Nevertheless it can be assumed that the effect of wall roughness on the loss coefficient was adequately estimated.

**Acknowledgements** The research was partially supported by grant projects No. 103/09/0977 and P101/10/1230 of the Czech Science Foundation and by the Research Plans No. AV0Z20760514 and MSMT6840770010.

## References

1. Ulrych, J., Benetka, J., Jelínek, T., Valenta, R., Tajč, L.: Experimental research of surface roughness impact on transonic flow in blade cascades, In: Proc. XVIII Symposium on Measuring Techniques in Turbomachinery, Thessaloniki, CD-ROM 7 p. (2006)
2. Louda P., Kozel K., Příhoda J.: Computation of turbulent compressible and incompressible flows. In: 8th International Symposium on Experimental and Computational Aerothermodynamics of Internal Flows, Lyon (2007)

3. Aupoix B., Spalart P.R.: Extension of the Spalart-Allmaras turbulence model to account for wall roughness, Int. J. Heat and Fluid Flow, **24**, 454–462 (2003)
4. Menter F. R.: Two-Equations Eddy-Viscosity Turbulence Models for Engineering Applications, AIAA J., Vol.32, **8**, 1598–1605 (1994)
5. Hellsten, A.: New advanced $k$-$\omega$ turbulence model for high-lift aerodynamics, AIAA J., **43**, 1857–1869 (2005)
6. Hellsten A., Laine S.: Extension of the $k$-$\omega$ SST turbulence model for flows over rough walls, AIAA Paper 97–3577 (1997)
7. Liou M.-S.: On a new class of flux splittings. Lecture Notes in Phys., **414**, 115–119 (1993)
8. Louda P., Kozel K., Příhoda J.: Numerical solution of 2D and 3D viscous incompressible steady and unsteady flows using artificial compressibility method. Int. J. for Numerical Methods in Fluids, **56**, 1399–1407 (2008)
9. Nikuradse J.: Strömungsgesetze in rauhen Rohren, VDI-Forschungsheft 361 (1933) (or NACA TM-1292, 1965)
10. Pimenta, M.M., Moffat, R.J., Kays, W.M.: The structure of a boundary layer on a rough wall with blowing and heat transfer, Jour. Heat Transfer, **101**, 193–198 (1979)
11. Song, S., Eaton, J.K.: The effects of wall roughness on the separated flow over a smoothly contoured ramp, Experiments in Fluids, **33**, 38–46 (2002)
12. Wilcox, D.: Reassessment of the scale-determining equation, AIAA J., **26**, 1299–1310 (1988)
13. Wallin, S.: Engineering turbulence modeling for CFD with a focus on explicit algebraic Reynolds stress models, PhD thesis, Royal Institute of Technology, Stockholm (2000)